Acta Crystallographica Section C
Crystal Structure Communications
ISSN 0108-2701

A pair of diastereomeric 1:2 salts of (*R*)- and (*S*)-2-methylpiperazine with (2*S*,3*S*)-tartaric acid

Hiroshi Katagiri,[a]* Masao Morimoto[b] and Kenichi Sakai[b]

[a]Department of Chemistry and Chemical Engineering, Graduate School of Science and Engineering, Yamagata University, 4-3-16 Jonan, Yonezawa, Yamagata 992-8510, Japan, and [b]Specialty Chemicals Technology Development Department, Toray Fine Chemicals Co. Ltd, Minato-ku, Nagoya, Aichi 455-8502, Japan
Correspondence e-mail: kgri7078@yz.yamagata-u.ac.jp

Received 30 September 2009
Accepted 4 November 2009
Online 12 December 2009

The crystal structures of a pair of diastereomeric 1:2 salts of (*R*)- and (*S*)-2-methylpiperazine with (2*S*,3*S*)-tartaric acid, namely (*R*)-2-methylpiperazinediium bis[hydrogen (2*S*,3*S*)-tartrate] monohydrate, (I), and (*S*)-2-methylpiperazinediium bis[hydrogen (2*S*,3*S*)-tartrate] monohydrate, (II), both $C_5H_{14}N_2^{2+}\cdot 2C_4H_5O_6^-\cdot H_2O$, each reveal the formation of well-defined head-to-tail-connected hydrogen tartrate chains; these chains are linked into a two-dimensional sheet *via* intermolecular hydrogen bonds involving hydroxy groups and water molecules, resulting in a layer structure. The (*R*)-2-methylpiperazinediium ions lie between the hydrogen tartrate layers in the most stable equatorial conformation in (I), whereas in (II), these ions are in an unstable axial position inside the more interconnected layers and form a larger number of intermolecular hydrogen bonds than are observed in (I).

Comment

Tartaric acid is one of the most readily available enantiomerically pure compounds, and is potentially useful as an achiral resolving reagent for racemic amines (Gawronski & Gawronska, 1999). In diastereomeric salts consisting of chiral amines and tartaric acids, the hydrogen tartrate ion is often connected by an intermolecular hydrogen bond to the carboxylate group from another carboxylic acid to afford a one-dimensional chain structure, which leads to the construction of a two-dimensional sheet formed *via* intermolecular hydrogen bonds between hydroxy groups (Ryttersgaard & Larsen, 1998). Moreover, the chiral environment created by the layer of hydrogen tartrate ions is assumed to discriminate between the two ammonium enantiomers inside the layer, thus organizing the layer structure for the target amines (Bruun & Larsen, 1999; Sakurai *et al.*, 2006). To evaluate their potential for use in this way, we report here the crystal structures of a pair of diastereomeric 1:2 salts, (I) and (II), of (2*S*,3*S*)-tartaric acid with (*R*)- and (*S*)-2-methylpiperazine, respectively.

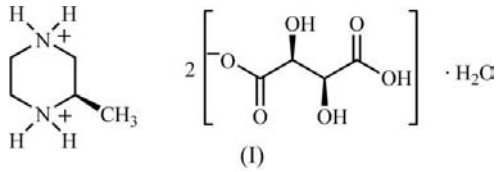

(I)

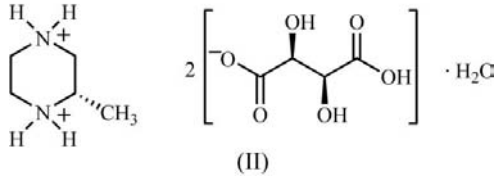

(II)

In the crystal structures of both compounds, the N atoms of the 2-methylpiperazine molecule each have two H atoms, showing that these amines are completely converted to quaternary ammonium cations (Figs. 1 and 2). The C1—N2—C4—C5 and N1—C3—C4—C5 torsion angles (Tables 1 and 3) indicate that the methyl groups are in the most stable equatorial position in the chair conformation of the piperazine ring in (I), whereas in (II), the methyl groups are in unstable axial positions. Although all the tartaric acid is present as tartrate in the 1:1 salts (Katagiri *et al.*, 2009), it is found that the two independent tartaric acid units are present as hydrogen tartrate ions in (I) and (II), owing to the loss of a single H atom. The conformations of the hydrogen tartrate ions have roughly the same geometry around the C7—C8 and C11—C12 axes; the relevant torsion angles are given in Tables 1 and 3. The present structures of both (I) and (II) conform to the general structure for hydrogen tartrate salts, namely, the hydrogen tartrate ions form a one-dimensional chain structure (Figs. 3 and 4) connected by strong negative-charge-assisted hydrogen bonds [(−)CAHB; Gilli *et al.*, 1994] [O5—H5*A*···O7^{ii} and O9—H9*A*···O12^{iii} in (I), and O5—H5*A*···O8^{v} and O9—H9*A*···O11^{viii} in (II); geometric details and symmetry codes are given in Tables 2 and 4]. These two symmetrically independent chains are, however, skew lines that are orthogonal to each other, unlike in the case of most frequently reported types (Bruun & Larsen, 1999).

Strong intermolecular O—H···O and N—H···O hydrogen bonds are observed and, particularly, the piperadinediium ions are tightly hydrogen bonded to water molecules and hydrogen tartrate ions in both (I) and (II) (Figs. 5 and 6, and Tables 2 and 4). The solubility of 12.7 g/100 g H_2O for (I) is less than that of 33.0 g/100 g H_2O for (II) at 303 K, and the crystal density of 1.582 Mg m^{-3} for (I) is slightly greater than that of 1.573 Mg m^{-3} for (II). The high packing efficiency of (I) is also evident in its higher 'packing coefficient' (Spek, 2009) (75.7%), which differs by just 0.5% from the value found for (II) (75.2%), indicating that the less soluble salt (I) has a slight advantage in close packing. In contrast, there are more hydrogen bonds in the more soluble salt (II) than in the less

  doi:10.1107/S0108270109046460

soluble salt (I), indicating the same behavior as has been observed for 1:1 salts (Katagiri *et al.*, 2009). The large number of hydrogen bonds in (II) is attributed to the contribution of the hydrogen bonds around the N atoms in the piperazinediium ions (Figs. 7 and 8). Furthermore, the melting point of 460–461 K for (II) is higher than that of 455–456 K for (I), also suggesting that the more soluble salt (II) is stabilized to a greater extent by intermolecular hydrogen bonds.

In the less soluble salt (I), the hydrogen tartrate chains construct a two-dimensional sheet *via* intermolecular hydrogen bonds with the hydroxy groups, leading to the formation of a layer structure. No interaction is observed between the hydrogen tartrate layers (Fig. 5). The piperazinediium ions lie between the hydrogen tartrate layers in the most stable equatorial conformation, anchored by five intermolecular hydrogen bonds formed by two tartrate ions and two water molecules (Fig. 7). The water molecules fill the structural void between the hydrogen tartrate layers. In contrast to the structure of (I), there are two independent forms of assembly of the hydrogen tartrate ions in the more soluble salt (II), and the layers are more interconnected (Fig. 6). One type of hydrogen tartrate chain is assembled by hydrogen bonds with the hydroxy groups to create a double-chain unit; no hydrogen bonds are formed between these

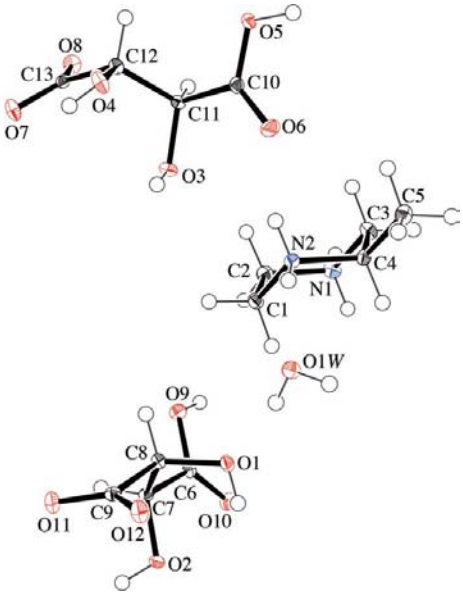

Figure 1
The asymmetric unit of (I), showing 50% probability displacement ellipsoids. H atoms are shown as spheres.

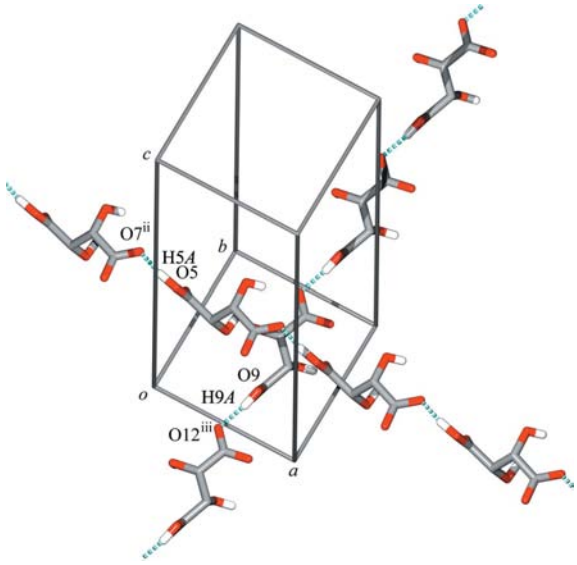

Figure 3
Head-to-tail-connected hydrogen tartrate chains in (I), showing the adoption of mutually orthogonal skew lines. (Symmetry codes as in Table 2.)

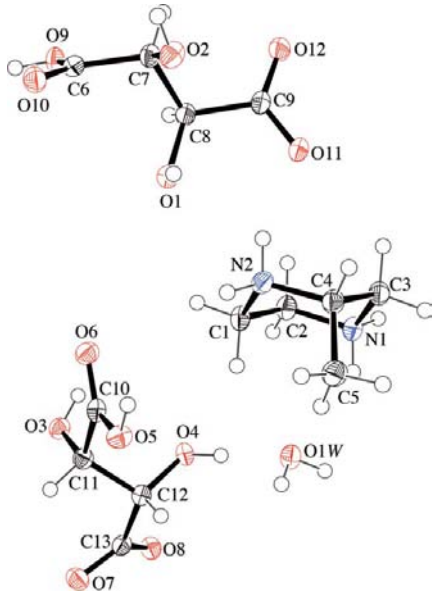

Figure 2
The asymmetric unit of (II), showing 50% probability displacement ellipsoids. H atoms are shown as spheres.

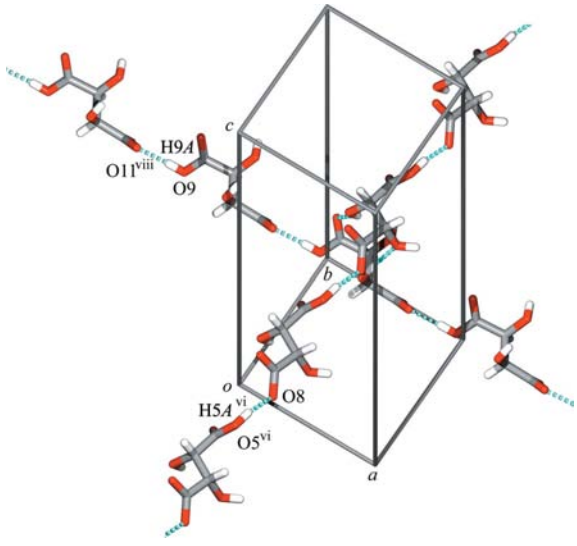

Figure 4
Head-to-tail-connected hydrogen tartrate chains in (II), showing the adoption of mutually orthogonal skew lines. (Symmetry codes as in Table 4.)

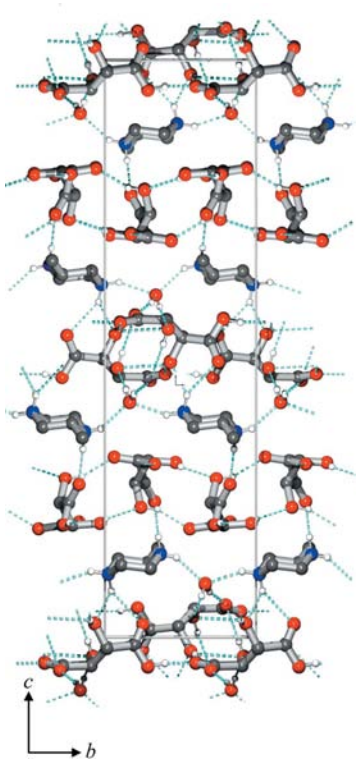

Figure 5
The packing of (I) along the *a* axis, showing the regular layers of hydrogen tartrate and piperazinediium ions interconnected in the equatorial position by hydrogen bonds.

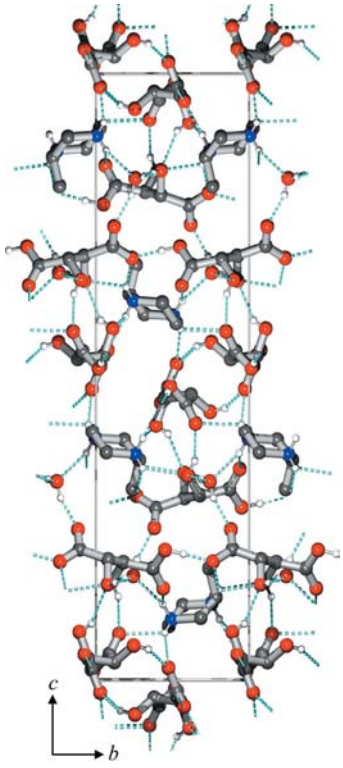

Figure 6
The packing of (II) along the *a* axis, showing the greater number of interconnected layers of hydrogen tartrate and piperazinediium ions interconnected in the axial position by hydrogen bonds.

double chains. The other type forms a sheet structure by hydrogen bonding *via* water molecules. Moreover, there are obvious hydrogen bonds between the hydrogen tartrate sheets, indicating that the layer-to-layer spacing is narrower than that in (I). The piperazinediium ions lie between the hydrogen tartrate layers in an unstable axial conformation, which is stabilized by eight intermolecular hydrogen bonds constructed of five tartrate ions and a water molecule (Fig. 8). These hydrogen bonds are bifurcated and are thus estimated to be weaker than those of ordinary hydrogen bonds formed by a single donor and acceptor. The water molecules behave as a hinge for the sheet structure of the hydrogen tartrate. The more soluble salt (II) is structurally disadvantaged in close packing, and adopts a less dense structure supported by intermolecular hydrogen bonds. These structural properties were similar to those of 1:1 salts.

The large contribution of the hydrogen bonds in the salt (II) showed a slight advantage of enthalpies. On the other hand, it has been reported that a comparison of vibrational move-

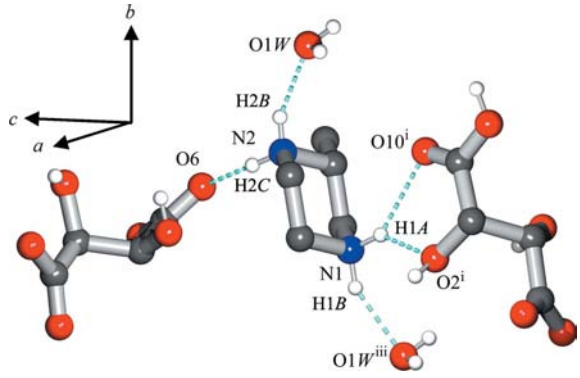

Figure 7
A perspective view of the partial packing of (I), showing the piperazinediium ions lying in the most stable equatorial conformation, stabilized by five intermolecular hydrogen bonds formed of two tartrate ions and two water molecules. (Symmetry codes as in Table 2.)

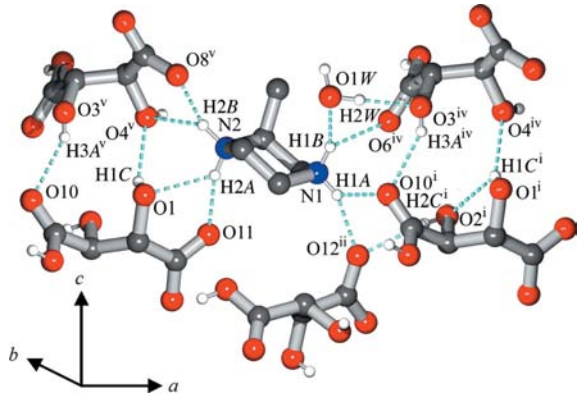

Figure 8
A perspective view of the partial packing of (II), showing how the piperazinediium ions lie between the hydrogen tartrate layers in the unstable axial conformation, stabilized by eight intermolecular hydrogen bonds formed by five tartrate ions and a water molecule. (Symmetry codes as in Table 4.)

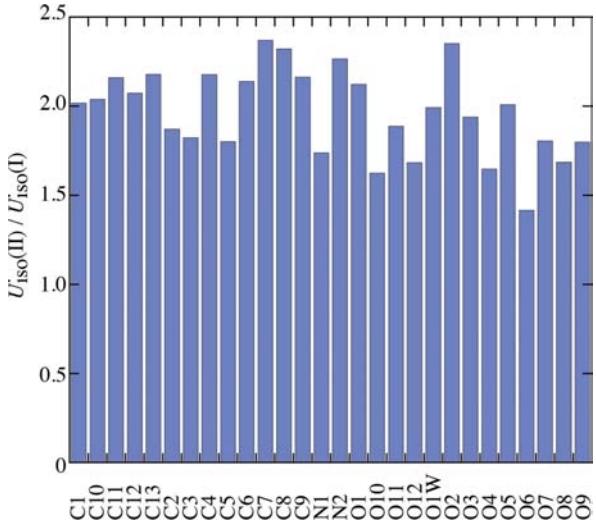

Figure 9
Ratios of the U_{eq} values for the same non-H atoms in (II) and (I).

ments observed as the U_{eq} values for all non-H atoms can be used in the calculation of solid-state entropies (Madsen & Larsen, 2007). The U_{eq} values of the salt (II) are almost double those in (I) (Fig. 9). These results demonstrate that the higher melting point of the less dense (II) is correlated not only with a difference in the enthalpies of the two compounds but also with that in their entropies.

Experimental

Enantiomerically pure (2*S*,3*S*)-tartaric acid and (*R*)- and (*S*)-2-methylpiperazine were manufactured by Toray Fine Chemicals Co. Ltd (Japan). Both title salts were prepared by heating 2 mmol of (2*S*,3*S*)-tartaric acid and 1 mmol of (*R*)-2-methylpiperazine [for (I)] or (*S*)-2-methylpiperazine [for (II)] under reflux in the smallest possible amount of water. Subsequent cooling to room temperature yielded a crop of colorless prisms [m.p. 455–456 K for (I) and 460–461 K for (II)]. The solubility of these salts in water was established by the equilibration method, *i.e.* by preparing a saturated solution at 303 K and determining its concentration by measuring the final weight of the salt dissolved in a saturated solution.

Compound (I)

Crystal data

$C_5H_{14}N_2^{2+}\cdot 2C_4H_5O_6^-\cdot H_2O$
M_r = 418.36
Orthorhombic, $P2_12_12_1$
a = 7.5571 (2) Å
b = 7.7903 (3) Å
c = 29.8324 (8) Å
V = 1756.30 (9) Å^3
Z = 4
Mo $K\alpha$ radiation
μ = 0.14 mm^{-1}
T = 108 K
0.60 × 0.60 × 0.60 mm

Data collection

Rigaku R-AXIS RAPID diffractometer
Absorption correction: multi-scan (*ABSCOR*; Higashi, 1995)
T_{min} = 0.919, T_{max} = 0.919
26023 measured reflections
2331 independent reflections
2271 reflections with $I > 2\sigma(I)$
R_{int} = 0.024

Refinement

$R[F^2 > 2\sigma(F^2)]$ = 0.025
$wR(F^2)$ = 0.062
S = 1.11
2331 reflections
291 parameters
H atoms treated by a mixture of independent and constrained refinement
$\Delta\rho_{max}$ = 0.33 e Å^{-3}
$\Delta\rho_{min}$ = −0.19 e Å^{-3}

Table 1
Selected torsion angles (°) for (I).

C1—N2—C4—C5	−179.89 (13)	C6—C7—C8—C9	−175.83 (12)
N1—C3—C4—C5	−179.76 (12)	O3—C11—C12—O4	67.41 (17)
O2—C7—C8—O1	68.02 (16)	C10—C11—C12—C13	176.33 (12)

Table 2
Hydrogen-bond geometry (Å, °) for (I).

D—H···A	D—H	H···A	D···A	D—H···A
N1—H1A···O2^{i}	0.90 (2)	2.03 (2)	2.7484 (19)	136 (2)
N1—H1A···O10^{i}	0.90 (2)	2.39 (2)	3.1814 (19)	146 (2)
O1W—H1W···O11^{ii}	0.84 (2)	1.90 (2)	2.7227 (17)	168 (2)
N1—H1B···O1W^{iii}	0.92 (2)	2.01 (2)	2.8522 (19)	152.1 (19)
O1W—H2W···O1	0.87 (2)	1.99 (2)	2.8516 (17)	169 (2)
N2—H2A···O6	0.88 (2)	1.88 (2)	2.7285 (19)	160 (2)
N2—H2B···O1W	0.85 (2)	2.03 (2)	2.7906 (19)	149 (2)
O3—H3A···O8^{iv}	0.85 (2)	1.97 (2)	2.7661 (18)	156 (2)
O4—H4A···O3^{iv}	0.77 (2)	2.28 (2)	2.9474 (17)	146 (2)
O5—H5A···O7^{ii}	1.03 (2)	1.46 (2)	2.4814 (16)	172.3 (19)
O1—H1C···O11^{v}	0.82 (2)	2.14 (2)	2.9389 (17)	163 (2)
O2—H2C···O12^{vi}	0.86 (2)	1.78 (2)	2.6249 (17)	165 (2)
O9—H9A···O12^{iii}	0.91 (2)	1.69 (2)	2.5878 (17)	169 (2)

Symmetry codes: (i) $x-\frac{1}{2}, -y+\frac{1}{2}, -z$; (ii) $x-1, y, z$; (iii) $x, y-1, z$; (iv) $-x+1, y+\frac{1}{2}, -z+\frac{1}{2}$; (v) $x-\frac{1}{2}, -y+\frac{3}{2}, -z$; (vi) $x+\frac{1}{2}, -y+\frac{3}{2}, -z$.

Compound (II)

Crystal data

$C_5H_{14}N_2^{2+}\cdot 2C_4H_5O_6^-\cdot H_2O$
M_r = 418.36
Orthorhombic, $P2_12_12_1$
a = 7.6062 (3) Å
b = 7.6426 (3) Å
c = 30.3987 (11) Å
V = 1767.11 (12) Å^3
Z = 4
Mo $K\alpha$ radiation
μ = 0.14 mm^{-1}
T = 103 K
0.60 × 0.50 × 0.30 mm

Data collection

Rigaku R-AXIS RAPID diffractometer
Absorption correction: multi-scan (*ABSCOR*; Higashi, 1995)
T_{min} = 0.920, T_{max} = 0.959
27022 measured reflections
2342 independent reflections
2193 reflections with $I > 2\sigma(I)$
R_{int} = 0.063

Refinement

$R[F^2 > 2\sigma(F^2)]$ = 0.035
$wR(F^2)$ = 0.088
S = 1.07
2342 reflections
291 parameters
H atoms treated by a mixture of independent and constrained refinement
$\Delta\rho_{max}$ = 0.28 e Å^{-3}
$\Delta\rho_{min}$ = −0.18 e Å^{-3}

Table 3
Selected torsion angles (°) for (II).

C1—N2—C4—C5	−73.8 (2)	C6—C7—C8—C9	173.82 (18)
N1—C3—C4—C5	72.4 (3)	O4—C12—C11—O3	58.0 (2)
O2—C7—C8—O1	61.2 (2)	C13—C12—C11—C10	171.88 (18)

Table 4
Hydrogen-bond geometry (Å, °) for (II).

D—H···A	D—H	H···A	D···A	D—H···A
N1—H1A···O10^{i}	0.89 (3)	2.31 (3)	2.846 (3)	119 (3)
N1—H1A···O12^{ii}	0.89 (3)	1.96 (3)	2.770 (3)	150 (3)
N1—H1B···O1W	0.90 (3)	2.25 (3)	3.007 (3)	141 (3)
N1—H1B···O6^{iii}	0.90 (3)	2.27 (3)	2.817 (3)	118 (2)
O1—H1C···O4^{iv}	0.77 (3)	2.30 (3)	2.972 (2)	148 (3)
O1W—H1W···O7^{v}	0.84 (3)	1.82 (3)	2.637 (2)	163 (3)
N2—H2A···O1	0.90 (3)	2.26 (3)	2.846 (3)	122 (2)
N2—H2A···O11	0.90 (3)	1.96 (3)	2.820 (3)	159 (3)
N2—H2B···O4^{iv}	0.98 (3)	2.20 (3)	2.914 (3)	129 (2)
N2—H2B···O8^{iv}	0.98 (3)	1.85 (3)	2.732 (3)	149 (3)
O2—H2C···O12^{vi}	0.83 (4)	2.19 (4)	2.909 (2)	145 (3)
O1W—H2W···O3^{iii}	0.87 (4)	1.87 (4)	2.736 (2)	171 (3)
O3—H3A···O10^{vii}	0.83 (3)	2.22 (3)	2.797 (2)	126 (3)
O4—H4A···O1W	0.89 (4)	1.79 (4)	2.679 (2)	174 (3)
O5—H5A···O8^{iv}	0.94 (3)	1.59 (3)	2.527 (2)	171 (4)
O9—H9A···O11^{viii}	0.84 (4)	1.72 (4)	2.553 (3)	177 (3)

Symmetry codes: (i) $x+1, y-1, z$; (ii) $x+\frac{1}{2}, -y+\frac{3}{2}, -z$; (iii) $x+1, y, z$; (iv) $x, y+1, z$; (v) $-x+1, y+\frac{1}{2}, -z+\frac{1}{2}$; (vi) $x-\frac{1}{2}, -y+\frac{5}{2}, -z$; (vii) $x, y-1, z$; (viii) $x-1, y, z$.

In the refinement of both (I) and (II), H atoms attached to O and N atoms were located by difference Fourier analysis and their positions refined with U_{iso}(H) values of $1.5U_{eq}$(N,O). The positions of other H atoms were calculated geometrically and refined as riding, with C—H bond lengths of 0.98–1.00 Å, and with U_{iso}(H) values of $1.2U_{eq}$(C) or $1.5U_{eq}$(methyl C). In both (I) and (II), in the absence of significant anomalous scattering effects, Friedel pairs were merged, and the absolute configuration assigned from the known configuration of (2*S*,3*S*)-tartaric acid.

For both compounds, data collection: *PROCESS-AUTO* (Rigaku, 1998); cell refinement: *PROCESS-AUTO*; data reduction: *CrystalStructure* (Rigaku/MSC, 2003); program(s) used to solve structure: *SHELXS97* (Sheldrick, 2008); program(s) used to refine structure: *SHELXL97* (Sheldrick, 2008); molecular graphics: *ORTEPIII* (Burnett & Johnson, 1996) and *PLATON* (Spek, 2009); software used to prepare material for publication: *Yadokari-XG 2009* (Wakita, 2001; Kabuto *et al.*, 2009).

Supplementary data for this paper are available from the IUCr electronic archives (Reference: EG3031). Services for accessing these data are described at the back of the journal.

References

Bruun, R. M. & Larsen, S. (1999). *Acta Cryst.* C**55**, 956–958.
Burnett, M. N. & Johnson, C. K. (1996). *ORTEPIII*. Report ORNL-6895. Oak Ridge National Laboratory, Tennessee, USA.
Gawronski, J. & Gawronska, K. (1999). In *Tartaric and Malic Acids in Synthesis: A Source Book of Building Blocks, Ligands, Auxiliaries and Resolving Agents*. New York, Chichester, Brisbane, Toronto: John Wiley and Sons.
Gilli, P., Bertolasi, V., Ferretti, V. & Gill, G. (1994). *J. Am. Chem. Soc.* **116**, 909–915.
Higashi, T. (1995). *ABSCOR*. Rigaku Corporation, Tokyo, Japan.
Kabuto, C., Akine, S., Nemoto, T. & Kwon, E. (2009). *J. Crystallogr. Soc. Jpn*, **51**, 218–224.
Katagiri, H., Morimoto, M. & Sakai, K. (2009). *Acta Cryst.* C**65**, o357–o360.
Madsen, A. Ø. & Larsen, S. (2007). *Angew. Chem. Int. Ed.* **46**, 8609–8613.
Rigaku (1998). *PROCESS-AUTO*. Rigaku Corporation, Tokyo, Japan.
Rigaku/MSC (2003). *CrystalStructure*. Version 3.6.0. Rigaku/MSC, The Woodlands, Texas, USA.
Ryttersgaard, C. & Larsen, S. (1998). *Acta Cryst.* C**54**, 1698–1701.
Sakurai, R., Yuzawa, A., Sakai, K. & Hirayama, N. (2006). *Cryst. Growth Des.* **6**, 1606–1610.
Sheldrick, G. M. (2008). *Acta Cryst.* A**64**, 112–122.
Spek, A. L. (2009). *Acta Cryst.* D**65**, 148–155.
Wakita, K. (2001). *Yadokari-XG*. http://www.hat.hi-ho.ne.jp/k-wakita/yadokari.